J. Am. Soc. Mass Spectrom. (2019) 30:1956–1963
DOI: 10.1007/s13361-019-02226-2

FOCUS: HONORING HELMUT SCHWARZ´S ELECTION TO THE NATIONAL ACADEMY OF SCIENCES: RESEARCH ARTICLE

Size-Dependent Association of Cobalt Deuteride Cluster Anions $Co_3D_n^-$ (n = 0–4) with Dinitrogen

Li-Hui Mou,[1,2,3] Zi-Yu Li,[1,3] Qing-Yu Liu,[1,3] Sheng-Gui He[1,2,3]

[1]State Key Laboratory for Structural Chemistry of Unstable and Stable Species, Institute of Chemistry, Chinese Academy of Sciences, Beijing, 100190, People's Republic of China
[2]University of Chinese Academy of Sciences, Beijing, 100049, People's Republic of China
[3]CAS Research/Education Center of Excellence in Molecular Sciences, Beijing National Laboratory for Molecular Sciences, Beijing, 100190, People's Republic of China

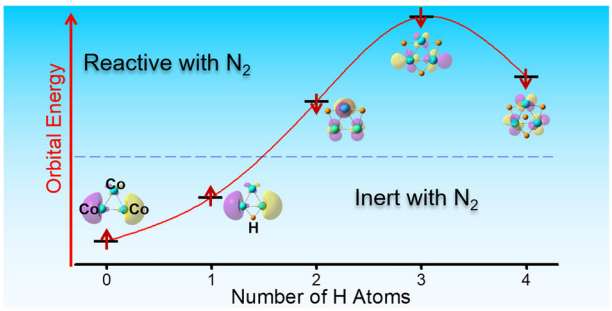

Abstract. Dinitrogen (N_2) activation by metal hydride species is of fundamental interest and practical importance while the role of hydrogen in N_2 activation is not well studied. Herein, the structures of $Co_3D_n^-$ (n = 0–4) clusters and their reactions with N_2 have been studied by using a combined experimental and computational approach. The mass spectrometry experiments identified that the $Co_3D_n^-$ (n = 2–4) clusters could adsorb N_2 while the $Co_3D_n^-$ (n = 0 and 1) clusters were inert. The photoelectron imaging spectroscopy indicated that the electron detachment energies of $Co_3D_{2-4}^-$ are smaller than those of $Co_3D_{0,1}^-$, which characterized that it is easier to transfer electrons from $Co_3D_{2-4}^-$ than from $Co_3D_{0,1}^-$ to activate N_2. The density functional theory calculations generally supported the experimental observations. Further analysis revealed that the H atoms in the $Co_3H_n^-$ (n = 2–4) clusters generally result in higher energies of the Co 3*d* orbitals in comparison with the $Co_3H_n^-$ (n = 0 and 1) systems. By forming chemical bonds with H atoms, the Co atoms of $Co_3H_{2-4}^-$ are less negatively charged with respect to the naked Co_3^- system, which leads to higher N_2 binding energies of $Co_3H_{2-4}N_2^-$ than that of $Co_3N_2^-$.

Keywords: Ion-molecule reactions, Mass spectrometry, Photoelectron imaging spectroscopy, N_2 activation, Cobalt, Density functional theory

Received: 24 February 2019/Revised: 8 April 2019/Accepted: 10 April 2019/Published Online: 24 June 2019

Introduction

Mild, energy-saving approaches for conversion of N_2 into available nitrogenous species are highly desirable in view of enormous energy consumption and greenhouse gas production in industrial Harber–Bosch process [1, 2]. Although the thermodynamically stable and kinetically inert N≡N bond renders its utilization a typically challengeable issue [3], some remarkable progress has been made on the daunting road of N_2 fixation in different research areas [4–8]. One thing in common is that the N_2 molecule should interact with a metal system [4, 8], in most cases, with multiple metal sites [5–7]. Recently, the transition metal hydride complexes have attracted extensive attentions owing to the potential in direct reduction of N_2 avoiding the use of extra strong reducing agents and proton sources [9–12]. For example, a trinuclear titanium polyhydride complex found by Hou et al. can induce N_2 cleavage and hydrogenation at ambient conditions [10]. Besides, it is significant to study N_2 activation by hydride species because they are related to the Harber–Bosch process and biological nitrogen fixation [9, 13].

Gas-phase clusters are ideal models to mimic the active sites of related condensed-phase systems [14–18]. Homonuclear metal clusters such as M_{3-9}^- (M=Ni, Pd, Pt) [19], Nb_n^- (n = 2–7) [20], W_n (n = 4–26) [21], Co_n (n = 4–28) [22], Co_n^+(n =

Electronic supplementary material The online version of this article (https://doi.org/10.1007/s13361-019-02226-2) contains supplementary material, which is available to authorized users.

Correspondence to: Zi–Yu Li; *e-mail:* liziyu2010@iccas.ac.cn, Sheng–Gui He; *e-mail:* shengguihe@iccas.ac.cn

1–18) [23, 24], and Ta_2^+ [25] have been reported to adsorb N_2 in either a molecular or a dissociative way. The size-dependent reactivity and donation/back-donation of electrons in N_2 activation were uncovered. There have been some reports and knowledge of N_2 activation by metal clusters doped with ancillary main group atoms (C, S, etc.) in gas-phase investigations [26, 27]. However, to the best of our knowledge, there has been no report about the N_2 activation by gas-phase metal hydride species that have already been studied to activate other very stable molecules such as CO_2 [28–31] and CH_4 [32–35].

In this work, we studied the gas-phase reactions between polynuclear cobalt deuteride clusters anions $Co_3D_n^-$ ($n = 0$–4) and N_2 via mass spectrometry, photoelectron imaging spectroscopy, and quantum chemical calculations. Cobalt is a cheap, abundant, and monoisotopic (beneficial for mass spectrometry) late transition metal. Pure cobalt is less competitive than the early transition metals in N_2 activation due to the energetically lower *d* orbitals that can be inefficient in π-back-donation [36]. It can be intriguing and instructive to use hydrogen atoms to promote the reactivity of cobalt clusters in N_2 activation in terms of fundamental and practical aspects. The cobalt deuteride/hydride species (CoD^+, $CoH_{1,2}^-$) [37] have been generated in the gas phase while we are not aware of them being utilized in N_2 reactivity studies. It is noteworthy that a lot of effort has been devoted to studying the reactions of small molecules (H_2, N_2, CH_4, $C_2H_{2,4}$, and/or CO) with cobalt cluster systems Co_n ($n = 4$–28) [22], Co_n^+ ($n = 1$–18) [23, 24], and Co_nN ($n = 7$–9)[38]. The photoelectron spectroscopy of Co_n^- ($n = 1$–108) has also been investigated by Wang and his coworkers [39].

Experimental and Computational Methods

Experimental Methods

Details of the experimental setup can be found in our previous studies [40, 41], and only a brief outline of the experiments is given below. In the reactivity experiments, the $Co_3D_n^-$ ($n = 0$–4) cluster anions were generated by laser ablation of a rotating and translating cobalt metal disk in the presence of 10% D_2 seeded in a He carrier gas with a backing pressure of about 4 atm. The cluster anions of interest were mass-selected by a quadrupole mass filter (QMF) [40] and then entered into a linear ion trap (LIT) reactor [41], in which they were confined and thermalized by collisions with a pulse of He gas for about 1.4 ms. The thermalized cluster anions subsequently reacted with a pulse of N_2 for about 8.6 ms. The pressures of N_2 were in the range of 1–2 Pa. The reactant and product ions ejected from the LIT were transferred into a reflectron time-of-flight mass spectrometer (TOF-MS) for mass and intensity measurements [41].

The photoelectron imaging spectroscopy (PEIS) experiments were carried out with a separate apparatus of tandem TOF-MS coupled with an optical parametric oscillator (OPO) laser source and a PEIS system [42]. The $Co_3D_n^-$ ($n = 0$–4) clusters were generated according to the procedure described in the reactivity experiments with 5% D_2 (for $n = 3$ and 4) and 0.6% D_2 (for $n = 0$–2) seeded in He. The temperature of the cluster source was 298 K. The generated cluster anions from the supersonic expansion were skimmed into the tandem TOF-MS and were mass-selected by the primary TOF-MS with a mass gate to interact with a 550 nm laser beam delivered from the OPO system. The photodetached electrons were accelerated to the PEIS detector where the electron velocities were imaged. The two-dimensional images were transformed into three-dimensional electron velocity distributions. The photoelectron kinetic energies and angular distribution were obtained [43, 44]. The resolution of the photoelectron spectrometer was found to be around 30 meV for electrons with 1 eV kinetic energy in the test experiment with the gold anions [42].

Computational Methods

Density functional theory (DFT) calculations using Gaussian 09 program [45] were carried out to investigate the structures of $Co_3H_n^-$ ($n = 0$–4) as well as the mechanistic details for the size-dependent reactivity with N_2. There is a long-standing controversy on the most stable geometry of Co_3^-. The reported DFT calculations predicted either a linear or a triangular structure, depending on the functionals and basis sets adopted [46–51]. To find an appropriate functional for the polynuclear cobalt hydrides, the experimental values of electron detachment energies of Co_3^- [39], bond length of Co–Co [52], and bond dissociation energy of Co–H [53] were used to test various functionals (Table S1). It turned out that the TPSS functional [54] is the best overall with the def2-TZVP basis set [55]. The low-lying structure isomers for each of $Co_3H_n^-$ ($n = 0$–4) were determined by the TPSS calculations for different spin multiplicities. The electron adiabatic detachment energies (ADEs) and vertical detachment energies (VDEs) were calculated. Based on the structures of $Co_3H_n^-$ ($n = 0$–4), the structures and N_2 adsorption energies of $Co_3H_n(N_2)_x^-$ ($x = 1$, 2, or 3) were calculated. The reported relative energies of the cluster isomers were corrected with zero-point vibrations. The molecular orbital (MO) analysis and natural bond orbital (NBO) analysis were performed to further interpret the experimental results.

Results

Reactivity of $Co_3D_n^-$ ($n = 0$–4) with N_2

The TOF mass spectra for the interactions of $Co_3D_n^-$ ($n = 0$–4) with N_2 are shown in Figure 1. It is obvious that in the reactions of Co_3^- (Figure 1a) and Co_3D^- (Figure 1b) with N_2, no product peaks were generated. In contrast, under similar experimental conditions, the interactions of $Co_3D_2^-$ (Figure 1c), $Co_3D_3^-$ (Figure 1d), and $Co_3D_4^-$ (Figure 1e) with N_2 generated product peaks that can be assigned as $Co_3D_{2-4}N_2^-$, suggesting the following reaction channels:

$$Co_3D_{2-4}^- + N_2 \rightarrow Co_3D_{2-4}N_2^- \quad (1)$$

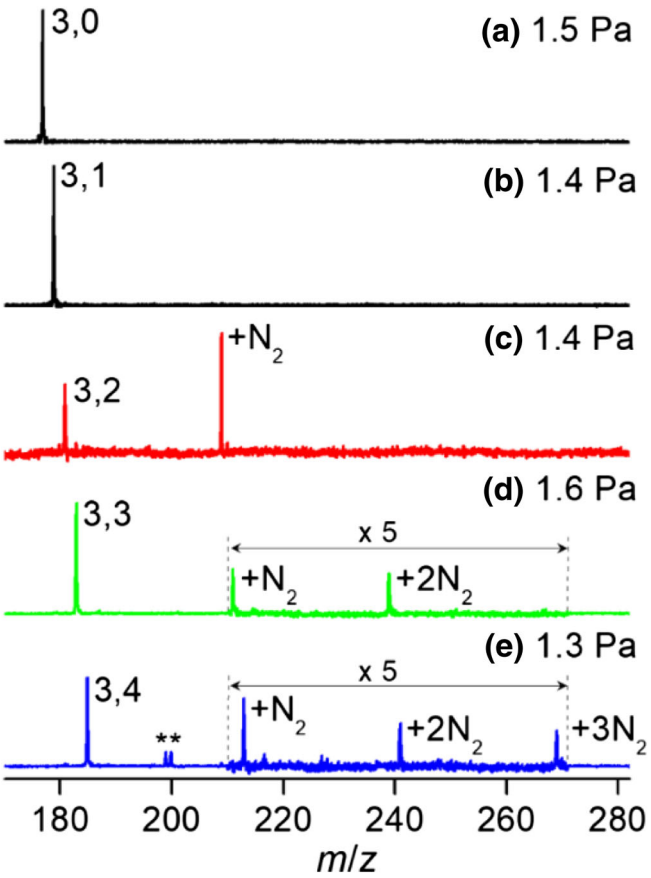

Figure 1. Time-of-flight mass spectra for the reactions of mass-selected (**a**) Co_3^-, (**b**) Co_3D^-, (**c**) $Co_3D_2^-$, (**d**) $Co_3D_3^-$, and (**e**) $Co_3D_4^-$ with 1.3–1.6 Pa N_2 for about 8.6 ms. Peaks marked with asterisks are due to the residual water in the gas handling system

In addition to the adsorption of one N_2 molecule, the adsorption of the second N_2 molecules on $Co_3D_{3,4}N_2^-$ appeared, indicating the following reaction channels:

$$Co_3D_{3,4}N_2^- + N_2 \rightarrow Co_3D_{3,4}(N_2)_2^- \quad (2)$$

The adsorption of the third N_2 molecule on $Co_3D_4(N_2)_2^-$ was also observed, corresponding to the following reaction channel:

$$Co_3D_4(N_2)_2^- + N_2 \rightarrow Co_3D_4(N_2)_3^- \quad (3)$$

The pseudo-first-order rate constants (k_1) of the reactions between $Co_3D_n^-$ ($n = 0$–4) clusters and N_2 were determined by Eq. (4) [56], in which I_R is the intensity of the reactant cluster ions after the reaction, I_T is the total ion intensity including product ion contribution, P is the effective pressure of the reactant gas, k_B is the Boltzmann constant, T is the temperature (298 K) of the reactant gas, and t_R is the reaction time (8.6 ms).

$$\ln\frac{I_R}{I_T} = -k_1\frac{P}{k_B T}t_R \quad (4)$$

When estimating the k_1 value in Eq. (4), the systematic deviations of t_R (± 3%), T (± 1%), and P (± 20%) were considered. As shown in Figure 2, the k_1 values for the reactions of $Co_3D_{2-4}^-$ with N_2 were determined to be $(3.4 \pm 0.7) \times 10^{-13}$, $(5.9 \pm 1.2) \times 10^{-14}$, and $(9.3 \pm 1.9) \times 10^{-14}$ cm^3 molecule^{-1} s^{-1}, respectively. The k_1 value of $Co_3D_2^-$ with N_2 is about six and four times larger than those of $Co_3D_3^-$ and $Co_3D_4^-$ systems, respectively.

DFT Calculated Structures and N_2 Adsorption Energies

The DFT calculated structures of the $Co_3H_n^-$ ($n = 0$–4) clusters and the N_2 adsorption products are presented in Figure 3 (see Figures S1 and S2 for more details). For clarity, the *i*th isomer of $Co_3H_n^-$ is denoted as ***n-i***. For example, **0–1** denotes the most stable structure of Co_3^-. Similarly, N_2 adsorption complex $Co_3H_n(N_2)_x^-$ is denoted as ***n-Cx-i***. The DFT calculated lowest-lying isomer of Co_3^- (**0–1**) has an equilateral triangular structure with the bond length of 226 pm and the nonet spin state, while the linear structure of Co_3^- (**0–2**) has the septet state that is 0.38 eV higher in energy than the triangular one. For Co_3H^-, the lowest-lying isomer (**1–1**) has the octet spin state and the C_s symmetry. The H atom in isomer **1–1** is bridgingly bonded with two Co atoms. The isomer **1–2** with a terminal H atom and the isomer **1–3** with the C_{2v} symmetry were calculated to be 0.11 and 0.19 eV higher in energy than the **1–1** structure, respectively. All of the H atoms in the lowest-lying isomers of $Co_3H_2^-$ (**2–1**) and $Co_3H_3^-$ (**3–1**) are bridgingly bonded. One of the four H atoms in $Co_3H_4^-$ (**4–1**) is terminally bonded. Each of the $Co_3H_n^-$ ($n = 1$–4) clusters has one or two isomers that are very close in energy (within 0.2 eV) to the lowest-lying isomers. These isomers are possible candidates that could be populated in the cluster source. It is noteworthy that test calculations indicated that the cluster structures with an unbroken H–H bond such as $(H_2)Co_3H^-$ and $(H_2)Co_3H_2^-$ are all high in energy (isomers **3–6** and **4–6** in Figure S1).

For the N_2 adsorption complexes, several N_2 binding modes were considered and it turned out that the end-on coordination is the most favorable mode. The most stable structures of the

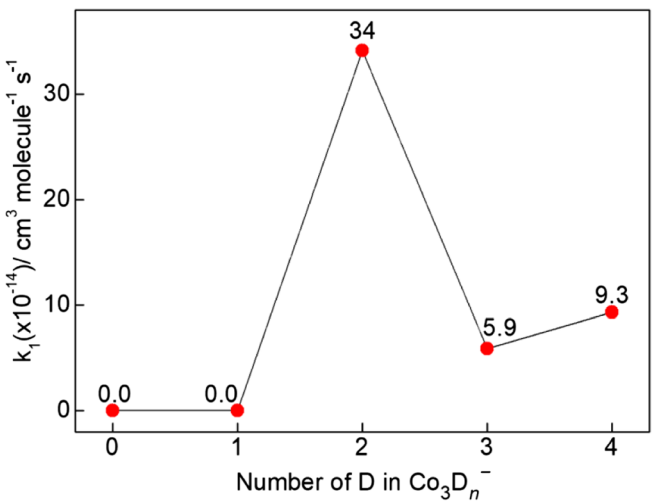

Figure 2. The pseudo-first-order rate constants (k_1) for the reactions of $Co_3D_n^-$ ($n = 0$–4) with N_2

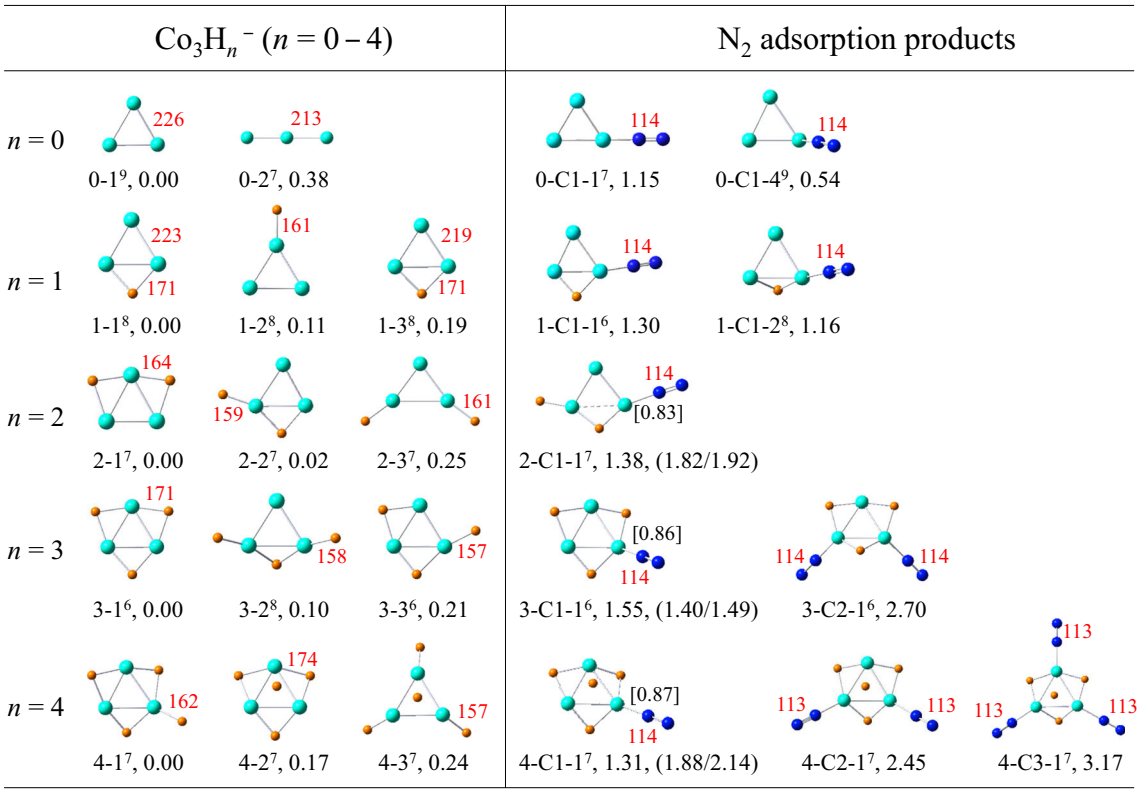

Figure 3. DFT calculated low-lying isomers of $Co_3H_n^-$ (n = 0–4) and their N_2 adsorption products. The relative energies with respect to the lowest-lying isomers (***n*-1**) for isomers (***n*-*i***) and the N_2 binding energies for adsorption products (***n*-C*x*-*i***) are in units of eV. Some selected bond lengths are given in pm. The superscripts indicate the spin multiplicities. The calculated ADE/VDE values of $Co_3H_nN_2^-$ (***n*-C1-1**, n = 2–4) are listed in the brackets. The bond orders of Co–N are listed in the square brackets

adsorption products $Co_3H_{2-4}N_2^-$ remain the same spin multiplicities as the reactant clusters while that of $Co_3H_{0,1}N_2^-$ have different spin multiplicities with respect to the reactants. As shown in Figure 3, the most stable structure of $Co_3N_2^-$ (**0-C1-1**) has the septet spin state and the N_2 adsorption energy (1.15 eV) is larger than that of the isomer (**0-C1-4**) with nonet spin state by 0.61 eV. For Co_3H^-, the low-lying isomers (**1-1**, **1-2**, and **1-3**) can bind N_2 to generate the most stable adsorption structure (**1-C1-1**) with the sextet spin state which has a larger adsorption (1.30 eV) energy than the isomer in the octet spin state (1.16 eV). For $Co_3H_2^-$, the low-lying isomers (**2-1**, **2-2**, and **2-3**) can adsorb N_2 to form the most stable adsorption structure (**2-C1-1**). For $Co_3H_3^-$, the N_2 adsorption onto **3-1** and **3-3** can produce the most stable complex **3-C1-1** while the complex formed from **3-2** with N_2 is higher in energy by 0.70 eV (**3-C1-3**, Figure S2). The most stable adsorption complex of $Co_3H_4N_2^-$ (**4-C1-1**) can be formed from **4-1** and **4-2** with N_2. In the adsorption complexes $Co_3H_2N_2^-$ (**2-C1-1**), $Co_3H_3N_2^-$ (**3-C1-1**), and $Co_3H_4N_2^-$ (**4-C1-1**), the bond orders (Figure 3, square brackets) between N_2 and the related Co atoms are around 0.83–0.87, which indicates that there is significant chemical bonding between N and Co atoms. Meanwhile the N-N bond order is decreased from 3.0 in free N_2 to about 2.5 in the association complexes. Therefore, the N-N bond was significantly activated in the adsorption complexes. The structures of the complexes with two and three N_2 molecules were also determined and all of the N_2 units are end-on coordinated (Figure 3, bottom right). The N_2 adsorption energy of $Co_3H_nN_2^-$ (***n*-C1-1**) generally increases as the increase of the number (n) of H atoms, which is qualitatively consistent with the experimental result that $Co_3H_{2-4}^-$ absorbed N_2 while $Co_3H_{0,1}^-$ did not (Figure 1).

Photoelectron Spectra and Structure Assignments

For most of the $Co_3H_n^-$ (n = 0–4) clusters, the DFT calculations predicted more than one isomeric structure that are close in energy (Figure 3, left). The PEIS experiment can be helpful to assign the cluster structures. The photoelectron spectra of $Co_3D_{0-4}^-$ are presented in Figure 4, and the experimental and DFT calculated ADE/VDE values are listed in Table 1. The simulated photoelectron spectra of the low-lying isomers of $Co_3H_n^-$ (n = 0–4) based on the generalized Koopmans' theorem [57], named as density of states (DOS) spectra, are presented in Figures S4–S8.

For Co_3^- (Figure 4a), the spectrum is dominated by a band ranging from about 1.40 to 1.80 eV, with a band center at the electron binding energy (EBE) of 1.62 eV, which determines the VDE value. The ADE value of Co_3^- was estimated to be 1.41 eV by extrapolating the lower EBE side of the band to zero photoelectron intensity. The ADE and VDE values (1.41/1.62 eV) of Co_3^- are in line with those (1.40/1.60 eV) of Wang

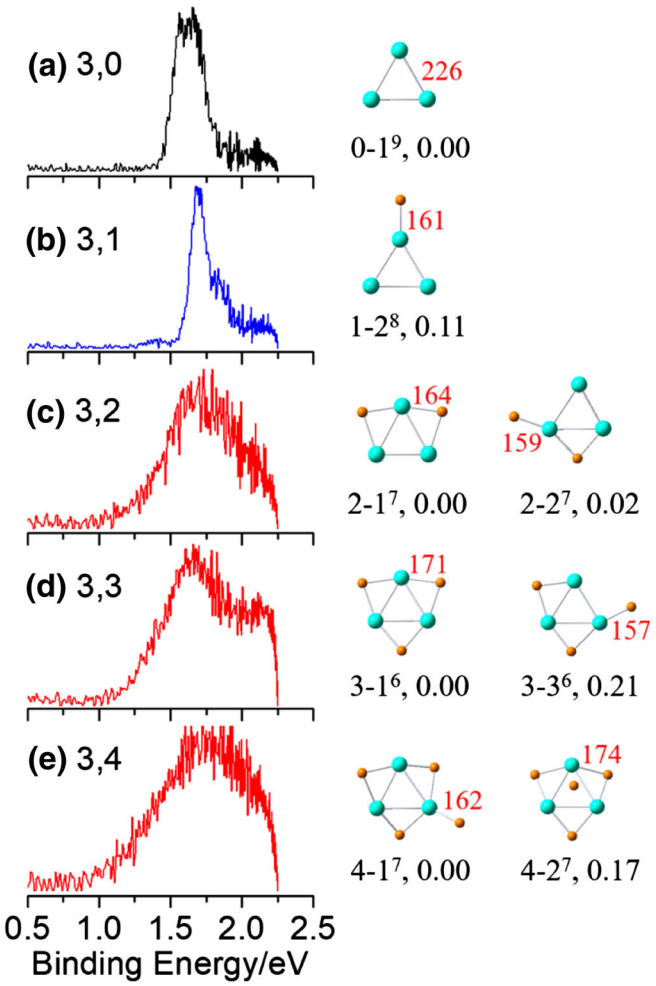

Figure 4. Photoelectron spectra of (**a**) Co_3^-, (**b**) Co_3D^-, (**c**) $Co_3D_2^-$, (**d**) $Co_3D_3^-$, and (**e**) $Co_3D_4^-$ taken with 550 nm (2.254 eV) photons. The structures shown are the most probable isomers in the experiments

and his coworkers in a previous study [39]. The DFT calculations predicted that the isomers **0-1** and **0-2** of Co_3^- have ADE/VDE values of 1.26/1.45 eV and 1.18/1.20 eV, respectively, and the former (1.26/1.45 eV) better matches the experiment (1.41/1.62 eV). Moreover, the DOS spectrum of isomer **0-1** can reproduce the experimental band position and pattern better than that of isomer **0-2** (Figure S4). Thus, the isomer **0-1** is assigned to be the most probable structure generated in the experiment. For Co_3D^-, the experimental ADE/VDE values are 1.57/1.69 eV (Figure 4b), which are slightly blue-shifted with respect to that of Co_3^- (1.41/1.62 eV). The theoretical ADE/VDE values of isomers **1-1**, **1-2**, and **1-3** are 1.22/1.23, 1.34/1.41, and 1.03/1.16 eV, respectively. Though isomer **1-1** was calculated to be the lowest-lying structure, its theoretical ADE/VDE values and DOS spectrum cannot fit the experiments well, while those of isomer **1-2** are closer to the experimental results (Figure S5). Isomer **1-3** is unlikely to be detected in the experiment because its theoretical ADE/VDE (1.03/1.16 eV) deviate largely from the experimental values (1.57/1.69 eV). Therefore, the isomer **1-2** is suggested to be the most probable structure contributing to the photoelectron spectrum of Co_3D^-.

In contrast to narrow spectral band of Co_3D^- and blue-shifted ADE of Co_3D^- with respect to that of Co_3^-, the spectral bands of $Co_3D_{2-4}^-$ (Figure 4c–e) are all broad and the ADE values of those clusters are all red-shifted (Table 1). For $Co_3D_2^-$, the isomers **2-1** and **2-2** are almost degenerate in energy (Figure 3). The combination of the DOS spectra of isomers **2-1** and **2-2** can fit most of the experimental features (Figure S6). Thus, isomers **2-1** and **2-2** are suggested to be coexist in the cluster source. Notably, the isomer **2-3** may have minor contribution because its DOS spectrum resembles the high EBE peaks in the experimental spectrum. Similarly, the broad spectral bands of $Co_3D_3^-$ by the experiment and the DOS spectra of several low-lying isomers (Figure S7) suggest that isomers **3-1** and **3-3** may be the major structures contributing to the experimental spectrum and isomer **3-2** may have the minor contribution. For $Co_3D_4^-$, the combination of the DOS spectra of isomers **4-1** and **4-2** (Figure S8) can match the experimental spectrum. The isomer **4-3** was unlikely to be touched in the PEIS experiments because the ADE/VDE values (2.72/3.06 eV) deviate largely from the experimental values (1.00/1.76 eV).

Discussion

Size-Dependent Reactivity of $Co_3D_n^-$ ($n = 0–4$) with N_2

The relaxed potential energy surface scans revealed that the processes of N_2 adsorption onto $Co_3D_{2-4}^-$ are exothermic and barrier-free and the N_2 adsorption energies of Co_3D_{2-4} N_2^- are generally larger (1.31–1.55 eV, Figure 3) than those of $Co_3N_2^-$ and $Co_3DN_2^-$. In addition, the spin conversions [58] have to take place in order to form the most stable structures of $Co_3N_2^-$ (**0-C1-1**) and $Co_3DN_2^-$ (**1-C1-1**). The relatively low N_2 binding energies of **0-C1-4** (0.54 eV) and **1-C1-2** (1.16 eV) and the possibly low-spin conversion efficiencies can lead to relatively weak N_2 adsorption, which is in agreement with no observation of $Co_3N_2^-$ and $Co_3DN_2^-$ in the experiment (Figure 1). Interestingly, the rate constant for the reaction of $Co_3D_3^-$ with N_2 is the smallest among $Co_3D_{2-4}^-$ reaction systems while $Co_3D_3N_2^-$ has a larger N_2 adsorption energy (1.55 eV) than $Co_3D_2N_2^-$ (1.38 eV) and $Co_3D_4N_2^-$ (1.31 eV). The DFT calculations indicated that the ADE (1.40 eV) and VDE (1.49 eV) values (Figure 3, in brackets) of $Co_3D_3N_2^-$ are smaller than the N_2 adsorption energy (1.55 eV), which means that associative electron detachment (AED) could take place in the experiment $Co_3D_3^- + N_2 \rightarrow (Co_3D_3N_2^-)^* \rightarrow Co_3D_3N_2 + e^-$. Note that the AED process was often observed in the reactions of small molecules with negative ions [59, 60]. In contrast, the AED process for the $Co_3D_2^-$ and $Co_3D_4^-$ reaction systems would not take place because the ADE values of $Co_3D_2N_2^-$ and $Co_3D_4N_2^-$ are significantly higher than the corresponding N_2 adsorption energies. In other words, $Co_3D_3^-$ could be the most reactive cluster towards N_2 but exhibited the smallest reaction rate among $Co_3D_{2-4}^-$ due to

the undetectable adsorption products (the I_T value in Eq. (4) could be underestimated for $Co_3D_3^- + N_2$).

The size-dependent reactivity of the $Co_3D_n^-$ ($n = 0$–4) clusters with N_2 is also supported by the PEIS experiment. The increased ADE of Co_3D^- (1.57 eV) with respect to that of Co_3^- (1.41 eV) indicates that it is more difficult for Co_3D^- to lose electrons to activate and then absorb N_2. In contrast, the decreased ADEs of $Co_3D_{2-4}^-$ (1.00–1.18 eV) mean that $Co_3D_{2-4}^-$ can lose electrons more easily to activate and then absorb N_2 than Co_3^- and Co_3D^-. Therefore, the different ADEs by the PEIS can generally interpret the size-dependent reactivity of the $Co_3D_n^-$ ($n = 0$–4) clusters with N_2 in the mass spectrometry experiment.

MO Analysis

To further understand the differences in electron detachment and N_2 adsorption energies of the $Co_3D_n^-$ ($n = 0$–4) clusters, the MO analysis has been performed. The highest occupied MOs (HOMOs) were considered to lose electrons in the electron detachment. The HOMOs of selected isomers of $Co_3H_{0-4}^-$ (note that the electronic structures of $Co_3H_{0-4}^-$ and $Co_3D_{0-4}^-$ are identical) are given in Figure 5. Note that both isomers **1-1** and **1-2** are listed for a comparison although the isomer **1-2** is assigned as the experimental species. It can be seen that both the number and the bonding mode of H atoms can influence the energies of HOMOs that are primarily composed of the Co 3*d* orbitals. A terminally bonded H atom (denoted as H_t) of Co_3H^- (**1-2**) lowers down the HOMO energy with respect to that of Co_3^-, which leads to a larger ADE of Co_3H^- (1.57 eV) than Co_3^- (1.41 eV). In contrast, the HOMO energy increases if the H atom is bridgingly bonded (denoted as H_b) in Co_3H^- (**1-1**). For $Co_3H_{2-4}^-$, the HOMO energies are all higher than that of Co_3^-, leading to smaller ADEs (1.00–1.18 eV) of $Co_3D_{2-4}^-$ than that of Co_3^-. The increased HOMO levels of $Co_3H_{2-4}^-$ can also facilitate back-donation bonding with the π^* orbitals of N_2 due to the decreased energy gap. Interestingly, for each of the $Co_3H_n^-$ ($n = 1$–4) clusters, the isomers with more H_b atoms tend to have higher HOMO levels.

NBO Analysis

The NBO analysis was performed to further interpret the bonding between N_2 and $Co_3H_n^-$ ($n = 0$–4) clusters, and the results are presented in Table 2. It turned out that the less negatively charged Co atom functions as the preferred trapping site to anchor N_2 molecule (hereafter called active-Co), while the other two Co atoms and the H atoms serve as indirect electron donors for the active-Co atom and N_2 molecule. The active-Co atoms in $Co_3H_{0,1}^-$ (**0-1** and **1-2**) have relatively large negative charges (−0.333 and −0.290 e, respectively) and more 4*s* electron occupancies ($4s^{1.32}$ and $4s^{1.31}$, respectively), which give rise to an unfavorable approach and relatively high σ-repulsion to the N_2 molecule. Upon bonding of two H atoms on the Co_3^- cluster to form $Co_3H_2^-$ (**2-1**), the natural charge on the active-Co increases to −0.099 e; meanwhile, more 3*d* and less 4*s* electron occupancies are located, which can result in an easier approach of N_2 to the cluster and a larger adsorption energy (1.38 eV). The above changes of charge on the active-Co and the electron occupancies in 3*d* and 4*s* orbitals are further enhanced when three H atoms are bonded with Co_3^- to form $Co_3H_3^-$ (**3-1**), which leads to a further larger N_2 adsorption energy (1.55 eV). For $Co_3H_4^-$, the natural charges on the active-Co and the four H atoms are +0.134 e and −1.225 e, respectively, and electron configuration of the 3*d* orbital reduces to $3d^{7.83}$. Such a positive Co site tends to compete with N_2 for electron densities. It turns out that the active-Co of $Co_3H_4^-$ (**4-1**) gains −0.250 e while the N_2 unit only gains −0.212 e which becomes smaller than the corresponding value (−0.259 e) of $Co_3H_3^-$ (**3-1**) reaction system. As a result, the N_2 is less activated in $Co_3H_4N_2^-$ (**4-C1-1**) than in $Co_3H_3N_2^-$ (**3-C1-1**), which is consistent with the larger N_2 adsorption energy of the latter (1.55 eV) versus the former (1.31 eV). One can conclude that the H atoms on the metal cluster (Co_3^-) significantly manipulate the charge/electron distribution (and the electronic structure), and an appropriate number of H atoms can enhance and maximize the cluster reactivity in N_2 activation.

Table 1. Experimental and DFT calculated ADE/VDE values of $Co_3D_n^-$ ($n = 0$–4)

n	Experimental ADE/VDE (eV)	Calculated ADE/VDE (eV)[a]		
0	1.41/1.62	*1.26/1.45 (0–1)*	1.18/1.20 (0–2)	
1	1.57/1.69	1.22/1.23 (1–1)	*1.34/1.41 (1–2)*	1.03/1.16 (1–3)
2	1.18/1.73	*1.21/1.25 (2–1)*	*0.93/1.47 (2–2)*	1.69/1.82(2–3)
3	1.10/1.66	*0.67/0.80 (3–1)*	0.57/1.97 (3–2)	*0.55/1.10 (3–3)*
4	1.00/1.76	*1.19/1.75 (4–1)*	*1.00/1.20 (4–2)*	2.72/3.06 (4–3)

[a]The isomers labeled in italics are the most probable isomers in the experiments

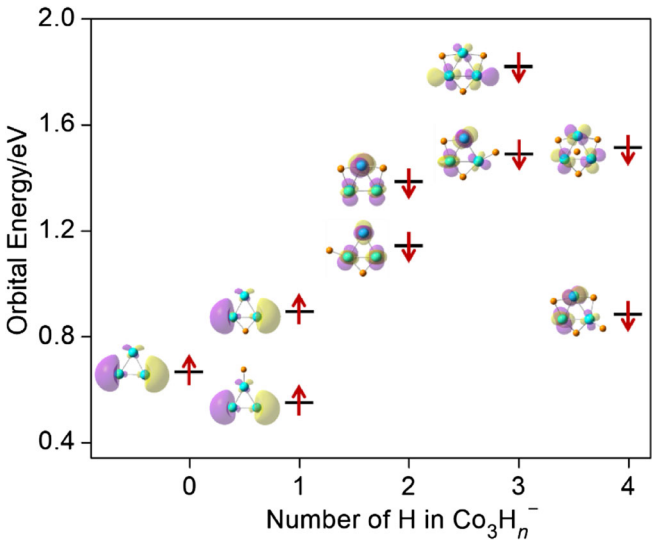

Figure 5. HOMO levels of selected $Co_3H_n^-$ ($n = 0$–4) cluster isomers that lose electrons to form the corresponding neutral counterparts. The up and down arrows denote the α and β electrons, respectively

Table 2. Natural charge and electron occupancy analysis

n-*i*[a]	Natural charge/e				Electron occupancy[d]
	Active-Co[b]	*n*H atoms[b]	N_2 unit[c]	Active-Co[c]	
0-1	−0.333				$4s^{1.32}\ 3d^{7.83}$
1-2	−0.290	−0.430			$4s^{1.31}\ 3d^{7.83}$
2-1	−0.099	−0.606	−0.256	−0.007	$4s^{0.93}\ 3d^{7.99}$
3-1	−0.007	−0.963	−0.259	−0.047	$4s^{0.61}\ 3d^{8.16}$
4-1	+0.134	−1.225	−0.212	−0.250	$4s^{0.58}\ 3d^{7.83}$

[a]The *i*th isomer of $Co_3H_n^-$ ($n = 0$–4)
[b]The natural charges on the active-Co (N_2 trapping site) and the H atoms
[c]The natural charges gained by the N_2 unit and the active-Co upon the process of N_2 adsorption
[d]The electron occupancy on the active-Co atom

Conclusion

The structures of $Co_3D_n^-$ ($n = 0$–4) clusters and their reactions with N_2 have been studied by mass spectrometry, photoelectron imaging spectroscopy, and density functional theory calculations. The $Co_3D_{2-4}^-$ clusters were observed to adsorb N_2 molecules in an ion trap reactor while Co_3^- and Co_3D^- were inert. The photoelectron spectra indicated that Co_3D^- and $Co_3D_{2-4}^-$ have blue- and red-shifted adiabatic electron detachment energies with respect to Co_3^-, which interprets the size-dependent abilities to transfer electrons from the cluster anions to activate and then absorb N_2 molecules. The density functional theory calculations revealed that (i) the disagreement of the largest N_2 adsorption energy and the smallest reaction rate of $Co_3D_3^-$ among $Co_3D_{2-4}^-$ reaction systems may be resulted from the exothermic process of the associative electron detachment, leading to the undetectable neutral product in the mass spectrometry experiment and the underestimate of the rate constant; (ii) the highest occupied molecular orbitals of $Co_3H_{2-4}^-$ (primarily Co 3*d* orbitals) are pushed higher in energy upon the bonding of H atoms on the Co_3^- cluster, which facilitates electron detachment as well as N_2 adsorption; and (iii) the bonding of H atoms on the Co_3^- cluster can also lead to less negatively charged Co sites with more 3*d* electron occupancies that are more effective to make π-back-donation bonding with N_2 molecules. An appropriate number of H (or D) atoms on a metal cluster such as Co_3^- can enhance and maximize the cluster reactivity in N_2 activation.

Acknowledgements

This work was supported by the National Natural Science Foundation of China (Nos. 21833011, 21773253, and 21603237).

References

1. Cherkasov, N., Ibhadon, A.O., Fitzpatrick, P.: A review of the existing and alternative methods for greener nitrogen fixation. Chem. Eng. Process. **90**, 24–33 (2015)
2. Pfromm, P.H.: Towards sustainable agriculture: Fossil-free ammonia. J. Renew. Sustain. Ener. **9**, 034702 (2017)
3. Tomaszewski, R.: Citations to chemical resources in scholarly articles: CRC Handbook of Chemistry and Physics and The Merck Index. Scientometrics. **112**, 1865–1879 (2017)
4. Avenier, P., Taoufik, M., Lesage, A., Solans-Monfort, X., Baudouin, A., de Mallmann, A., Veyre, L., Basset, J.M., Eisenstein, O., Emsley, L., Quadrelli, E.A.: Dinitrogen dissociation on an isolated surface tantalum atom. Science. **317**, 1056–1060 (2007)
5. Cui, X.-Y., Tang, C., Zhang, Q.: A review of electrocatalytic reduction of dinitrogen to ammonia under ambient conditions. Adv. Energy Mater. **8**, 1800369 (2018)
6. Zhang, N., Jalil, A., Wu, D.-X., Chen, S.-M., Liu, Y.-F., Gao, C., Ye, W., Qi, Z.-M., Ju, H.-X., Wang, C.-M., Wu, X.-J., Song, L., Zhu, J.-F., Xiong, Y.-J.: Refining defect states in $W_{18}O_{49}$ by Mo doping: A strategy for tuning N_2 activation towards solar-driven nitrogen fixation. J. Am. Chem. Soc. **140**, 9434–9443 (2018)
7. Liu, J.-C., Ma, X.-L., Li, Y., Wang, Y.-G., Xiao, H., Li, J.: Heterogeneous Fe_3 single-cluster catalyst for ammonia synthesis via an associative mechanism. Nat. Commun. **9**, 1610 (2018)
8. Wang, C.-X., Zhuang, J., Wang, G.-J., Chen, M.-H., Zhao, Y.-Y., Zheng, X.-M., Zhou, M.-F.: Tantalum dioxide complexes with dinitrogen. Formation and characterization of the side-on and end-on bonded $TaO_2(NN)_x$ ($x = 1-3$) complexes. J. Phys. Chem. A. **114**, 8083–8089 (2010)
9. Akagi, F., Matsuo, T., Kawaguchi, H.: Dinitrogen cleavage by a diniobium tetrahydride complex: Formation of a nitride and its conversion into imide species. Angew. Chem. Int. Ed. **46**, 8778–8781 (2007)
10. Shima, T., Hu, S.-W., Luo, G., Kang, X.-H., Luo, Y., Hou, Z.-M.: Dinitrogen cleavage and hydrogenation by a trinuclear titanium polyhydride complex. Science. **340**, 1549–1552 (2013)
11. Rittle, J., McCrory, C.C., Peters, J.C.: A 10^6-fold enhancement in N_2 binding affinity of an $Fe_2(\mu\text{-}H)_2$ core upon reduction to a mixed-valence $Fe^{II}Fe^{I}$ state. J. Am. Chem. Soc. **136**, 13853–13862 (2014)
12. Araake, R., Sakadani, K., Tada, M., Sakai, Y., Ohki, Y.: $[Fe_4]$ and $[Fe_6]$ hydride clusters supported by phosphines: Synthesis, characterization, and application in N_2 reduction. J. Am. Chem. Soc. **139**, 5596–5606 (2017)
13. Hoffman, B.M., Lukoyanov, D., Yang, Z.-Y., Dean, D.R., Seefeldt, L.C.: Mechanism of nitrogen fixation by nitrogenase: The next stage. Chem. Rev. **114**, 4041–4062 (2014)
14. Dillinger, S., Klein, M.P., Steiner, A., McDonald, D.C., Duncan, M.A., Kappes, M.M., Niedner-Schatteburg, G.: Cryo IR Spectroscopy of N_2 and H_2 on Ru_8^+: The Effect of N_2 on the H-Migration. J. Phys. Chem. Lett. **9**, 914–918 (2018)
15. Jiang, L.-X., Liu, Q.-Y., Li, X.-N., He, S.-G.: Design and application of a high-temperature linear ion trap reactor. J. Am. Soc. Mass Spectrom. **29**, 78–84 (2018)
16. Chen, Q., Zhao, Y.-X., Jiang, L.-X., Chen, J.-J., He, S.-G.: Coupling of methane and carbon dioxide mediated by diatomic copper boride cations. Angew. Chem. Int. Ed. **57**, 14134–14138 (2018)
17. Xue, W., Wang, Z.-C., He, S.-G., Xie, Y., Bernstein, E.R.: Experimental and theoretical study of the reactions between small neutral iron oxide clusters and carbon monoxide. J. Am. Chem. Soc. **130**, 15879–15888 (2008)
18. Fagiani, M.R., Song, X., Debnath, S., Gewinner, S., Schollkopf, W., Asmis, K.R., Bischoff, F.A., Muller, F., Sauer, J.: Dissociative water adsorption by $Al_3O_4^+$ in the gas phase. J. Phys. Chem. Lett. **8**, 1272–1277 (2017)
19. Hintz, P.A., Ervin, K.M.: Chemisorption and oxidation reactions of nickel group cluster anions with N_2, O_2, CO_2, and N_2O. J. Chem. Phys. **103**, 7897–7906 (1995)
20. Mwakapumba, J., Ervin, K.N.: Reactivity of niobium cluster anions with nitrogen and carbon monoxide. Int. J. Mass Spectrom. **161**, 161–174 (1997)
21. Mitchell, S.A., Rayner, D.M., Bartlett, T., Hackett, P.A.: Reaction of tungsten clusters with molecular nitrogen. J. Chem. Phys. **104**, 4012–4018 (1996)
22. Morse, M.D., Geusic, M.E., Heath, J.R., Smalley, R.E.: Surface reactions of metal clusters. II. Reactivity surveys with D_2,N_2, and CO. J. Chem. Phys. **83**, 2293–2304 (1985)
23. Nakajima, A., Kishi, T., Sone, Y., Nonose, S., Kaya, K.: Reactivity of positively charged cobalt cluster ions with CH_4, N_2, H_2, C_2H_4, and C_2H_2. Z. Phys. D: At., Mol. Clusters. **19**, 385–387 (1991)
24. Dillinger, S., Mohrbach, J., Hewer, J., Gaffga, M., Niedner-Schatteburg, G.: Infrared spectroscopy of N_2 adsorption on size selected cobalt cluster cations in isolation. Phys. Chem. Chem. Phys. **17**, 10358–10362 (2015)

25. Geng, C.-Y., Li, J.-L., Weiske, T., Schwarz, H.: Ta_2^+-mediated ammonia synthesis from N_2 and H_2 at ambient temperature. Proc. Natl. Acad. Sci. U. S. A. **115**, 11680–11687 (2018)
26. Mou, L.-H., Liu, Q.-Y., Zhang, T., Li, Z.-Y., He, S.-G.: Reactivity of tantalum carbide cluster anions TaC_n^- (n = 1–4) with dinitrogen. J. Phys. Chem. A. **122**, 3489–3495 (2018)
27. Heim, H.C., Bernhardt, T.M., Lang, S.M., Barnett, R.N., Landman, U.: Interaction of iron–sulfur clusters with N_2: Biomimetic systems in the gas phase. J. Phys. Chem. C. **120**, 12549–12558 (2016)
28. Zhang, X.-X., Liu, G.-X., Meiwes-Broer, K.H., Gantefor, G., Bowen, K.: CO_2 activation and hydrogenation by PtH_n^- cluster anions. Angew. Chem. Int. Ed. **55**, 9644–9647 (2016)
29. Zavras, A., Ghari, H., Ariafard, A., Canty, A.J., O'Hair, R.A.: Gas-phase ion-molecule reactions of copper hydride anions CuH_2^- and Cu_2H_3. Inorg. Chem. **56**, 2387–2399 (2017)
30. Jiang, L.-X., Zhao, C.-Y., Li, X.-N., Chen, H., He, S.-G.: Formation of gas-phase formate in thermal reactions of carbon dioxide with diatomic iron hydride anions. Angew. Chem. Int. Ed. **56**, 4187–4191 (2017)
31. Liu, Y.-Z., Jiang, L.-X., Li, X.-N., Wang, L.-N., Chen, J.-J., He, S.-G.: Gas-phase reactions of carbon dioxide with copper hydride anions $Cu_2H_2^-$: Temperature-dependent transformation. J. Phys. Chem. C. **122**, 19379–19384 (2018)
32. Liu, S.-L., Geng, Z.-Y., Wang, Y.-C., Yan, Y.-F.: Methane activation by MH^+ (M = Os, Ir, and Pt) and comparisons to the congeners of MH^+ (M = Fe, Co, Ni and Ru, Rh, Pd). J. Phys. Chem. A. **116**, 4560–4568 (2012)
33. Schlangen, M., Schroder, D., Schwarz, H.: Pronounced ligand effects and the role of formal oxidation states in the nickel-mediated thermal activation of methane. Angew. Chem. Int. Ed. **46**, 1641–1644 (2007)
34. Kretschmer, R., Schlangen, M., Schwarz, H.: Isomer-selective thermal activation of methane in the gas phase by $[HMO]^+$ and $[M(OH)]^+$ (M=Ti and V). Angew. Chem. Int. Ed. **52**, 6097–6101 (2013)
35. Zhang, Q., Michael, T.B.: Activation of methane by MH^+ (M = Fe, Co, and Ni): A combined mass spectrometric and DFT study. J. Phys. Chem. A. **108**, 9755–9761 (2004)
36. Holland, P.L.: Metal-dioxygen and metal-dinitrogen complexes: Where are the electrons? Dalton T. **39**, 5415–5425 (2010)
37. Miller, A.E.S., Feigerle, C.S., Lineberger, W.C.: Laser photoelectron-spectroscopy of MnH_2^-, FeH_2^-, CoH_2^-, and NiH_2^-: Determination of the electron-affinities for the metal dihydrides. J. Chem. Phys. **84**, 4127–4131 (1986)
38. Yin, S., Xie, Y., Bernstein, E.R.: Experimental and theoretical studies of ammonia generation: Reactions of H_2 with neutral cobalt nitride clusters. J. Chem. Phys. **137**, 124304 (2012)
39. Liu, S.-R., Zhai, H.-J., Wang, L.-S.: Electronic and structural evolution of Co_n clusters (n = 1–108) by photoelectron spectroscopy. Phys. Rev. B. **64**, 153402 (2001)
40. Wu, X.-N., Xu, B., Meng, J.-H., He, S.-G.: C–H bond activation by nanosized scandium oxide clusters in gas-phase. Int. J. Mass spectrom. **310**, 57–64 (2012)
41. Yuan, Z., Zhao, Y.-X., Li, X.-N., He, S.-G.: Reactions of $V_4O_{10}^+$ cluster ions with simple inorganic and organic molecules. Int. J. Mass spectrom. **354**, 105–112 (2013)
42. Liu, Q.-Y., Hu, L., Li, Z.-Y., Ning, C.-G., Ma, J.-B., Chen, H., He, S.-G.: Photoelectron imaging spectroscopy of MoC^- and NbN^-diatomic anions: A comparative study. J. Chem. Phys. **142**, 164301 (2015)
43. Neumark, D.M.: Slow electron velocity-map imaging of negative ions: Applications to spectroscopy and dynamics. J. Phys. Chem. A. **112**, 13287–13301 (2008)
44. Leon, I., Yang, Z., Liu, H.-T., Wang, L.-S.: The design and construction of a high-resolution velocity-map imaging apparatus for photoelectron spectroscopy studies of size-selected clusters. Rev. Sci. Instrum. **85**, 083106 (2014)
45. Frisch, M.J., Trucks, G.W., Schlegel, H.B., Scuseria, G.E., Robb, M.A., Cheeseman, J.R., Scalmani, G., Barone, V., Mennucci, B., Petersson, G.A., Nakatsuji, H., Caricato, M., Li, X., Hratchian, H.P., Izmaylov, A.F., Bloino, J., Zheng, G., Sonnenberg, J.L., Hada, M., Ehara, M., Toyota, K., Fukuda, R., Hasegawa, J., Ishida, M., Nakajima, T., Honda, Y., Kitao, O., Nakai, H., Vreven, T., Montgomery, J.A., Peralta Jr., J.E., Ogliaro, F., Bearpark, M., Heyd, J.J., Brothers, E., Kudin, K.N., Staroverov, V.N., Kobayashi, R., Normand, J., Raghavachari, K., Rendell, A., Burant, J.C., Iyengar, S.S., Tomasi, J., Cossi, M., Rega, N., Millam, J.M., Klene, M., Knox, J.E., Cross, J.B., Bakken, V., Adamo, C., Jaramillo, J., Gomperts, R., Stratmann, R.E., Yazyev, O., Austin, A.J., Cammi, R., Pomelli, C., Ochterski, J.W., Martin, R.L., Morokuma, K., Zakrzewski, V.G., Voth, G.A., Salvador, P., Dannenberg, J.J., Dapprich, S., Daniels, A.D., Farkas, Ö., Foresman, J.B., Ortiz, J.V., Cioslowski, J., Fox, D.J.: Gaussian 09, Revision A.1. Gaussian, Inc., Wallingford (2009)
46. Buendia, F., Beltran, M.R.: Theoretical study of hydrogen adsorption on Co clusters. Comput. Theor. Chem. **1021**, 183–190 (2013)
47. Bialach, P.M., Funk, A., Weiler, M., Gerhards, M.: IR spectroscopy on isolated Co_n(alcohol)$_m$ cluster anions (n = 1–4, m = 1–3): Structures and spin states. J. Chem. Phys. **133**, 194304 (2010)
48. Yoshida, H., Terasaki, A., Kobayashi, K., Tsukada, M., Kondow, T.: Spin-polarized electronic-structure of cobalt cluster anions studied by photoelectron-spectroscopy. J. Chem. Phys. **102**, 5960–5965 (1995)
49. Sebetci, A.: Cobalt clusters (Co_n, $n \leqslant 6$) and their anions. Chem. Phys. **354**, 196–201 (2008)
50. Pakiari, A.H., Dehghanpisheh, E.: The electronic structure of nanoparticle: Theoretical study of small cobalt clusters (Co_n , n = 2–5) (part A). Struct. Chem. **27**, 583–593 (2015)
51. Ma, Q.-M., Xie, Z., Wang, J., Liu, Y., Li, Y.-C.: Structures, stabilities and magnetic properties of small Co clusters. Phys. Lett. A. **358**, 289–296 (2006)
52. Kant, A., Strauss, B.H.: Dissociation energies of GeCu, GeCo, GeFe and GeCr. J. Chem. Phys. **49**, 3579 (1968)
53. Luo, Y.-R., Holmes, J.L.: The prediction of bond-dissociation energies for common organic-compounds. J. Mol. Struc-Theochem. **100**, 123–129 (1993)
54. Tao, J., Perdew, J.P., Staroverov, V.N., Scuseria, G.E.: Climbing the density functional ladder: Nonempirical meta-generalized gradient approximation designed for molecules and solids. Phys. Rev. Lett. **91**, 146401 (2003)
55. Weigend, F., Ahlrichs, R.: Balanced basis sets of split valence, triple zeta valence and quadruple zeta valence quality for H to R_n: Design and assessment of accuracy. Phys. Chem. Chem. Phys. **7**, 3297–3305 (2005)
56. Yuan, Z., Li, Z.-Y., Zhou, Z.-X., Liu, Q.-Y., Zhao, Y.-X., He, S.-G.: Thermal reactions of $(V_2O_5)_nO^-$ (n = 1–3) cluster anions with ethylene and propylene: Oxygen atom transfer versus molecular association. J. Phys. Chem. C. **118**, 14967–14976 (2014)
57. Tozer, D.J., Handy, N.C.: Improving virtual Kohn-Sham orbitals and eigenvalues: Application to excitation energies and static polarizabilities. J. Chem. Phys. **109**, 10180–10189 (1998)
58. Zhou, S.-D., Sun, X.-Y., Yue, L., Guo, C., Schlangen, M., Schwarz, H.: Selective nitrogen-atom transfer driven by a highly efficient intersystem crossing in the $CeON^+/CH_4$ system. Angew. Chem. Int. Ed. **57**, 15902–15906 (2018)
59. Xu, B., Zhao, Y.-X., Ding, X.-L., He, S.-G.: Reactions of $Sc_2O_4^-$ and $La_2O_4^-$ clusters with CO: A comparative study. Int. J. Mass Spectrom. **334**, 1–7 (2013)
60. Li, Y.-K., Wang, Z.-C., He, S.-G., Bierbaum, V.M.: Reactions of sulfur- and oxygen-containing anions with hydrogen atoms: A comparative study. J. Phys. Chem. Lett. **8**, 5725 (2017)